Highly stretchable graphene kirigami with tunable mechanical properties

Pan Shi [1], Yao Chen [1,2,*], Jian Feng [1], and Pooya Sareh [3,4]

[1] *Key Laboratory of Concrete and Prestressed Concrete Structures of Ministry of Education and National Prestress Engineering Research Center, Southeast University, Nanjing 211189, China*

[2] *School of Civil Engineering, Southeast University, Wuxi Campus, Wuxi 214082, China*

[3] *Creative Design Engineering Lab (Cdel), School of Engineering, Newcastle University, Newcastle upon Tyne, NE1 7RU, United Kingdom*

[4] *Escuela Técnica Superior de Ingeniería y Diseño Industrial, Universidad Politécnica de Madrid (UPM), Madrid 28012, Spain*

(Received 24 September 2023; revised 27 November 2023; accepted 12 February 2024; published 15 March 2024)

In recent years, kirigami techniques have inspired the design of graphene-based nanodevices with exceptional stretchability and ductility. Based on an I-shaped cutting pattern, here we propose a graphene kirigami that exhibits remarkable stretchability and ductility in two independent planar directions along with negative Poisson's ratios. The deformation mechanism underlying the high stretchability of the structure is the flipping and rotation of its cutting ligaments during elongation. Molecular dynamics simulations show that the yield and fracture strains of graphene kirigami can be enhanced by factors of 6 and 10 in the two planar directions. In addition, the mechanical properties of the graphene kirigami can be tuned by altering the cutting geometric parameters as well as incorporating distinct cutting patterns in series. We develop a numerical algorithm to predict the stress-strain response of the series-connected graphene kirigami, and verify its accuracy using appropriate simulations. On this basis, the stress-strain response of the series-connected graphene kirigami can be tuned by altering its geometric parameters and the number of building blocks. This graphene kirigami could be applied to the design and development of next-generation flexible electronics such as stretchable electrodes and strain sensors.

DOI: 10.1103/PhysRevE.109.035002

I. INTRODUCTION

Graphene is a classic two-dimensional material comprising one layer of sp^2-hybridized carbon arranged in a honeycomb lattice [1]. Owing to its exceptional thermoelectromechanical properties [2–4], graphene has found a diverse range of promising applications in the fields of nanoelectronics [5], energy storage devices [6], and nanosensors [7,8]. These nanodevices are often expected to maintain their functionality under large deformations or strains. However, graphene exhibits relatively low fracture strain and brittleness under tensile loads [9–11], limiting its potential applications to flexible nanodevices [12].

To date, various strategies have been proposed to impart high stretchability and ductility to graphene, among which "kirigami" (which combines "*kiri*" meaning "to cut" and "*kami*" meaning "paper") techniques have been proven to be experimentally feasible [13–16]. Employing parallel cutting patterns [17–19], Blees *et al.* [13] fabricated stretchable graphene kirigami transistors capable of maintaining their electrical properties over thousands of loading cycles.

Molecular dynamics (MD) simulations have demonstrated that the yield and fracture strains of this graphene kirigami exceed those of pristine graphene by several times [20–22]. The underlying mechanism involves the flipping and rotation of the interior cuts, a phenomenon arising when the edge and interior cuts overlap [20]. Nevertheless, the parallel-cut kirigami exhibits remarkable stretchability and ductility exclusively in the direction perpendicular to the cuts, while remaining brittle in the other planar direction. To address this issue, an effective strategy involves applying fractal-cut kirigami patterns featuring rotating units [23–26] to graphene. Several MD studies have shown that graphene kirigami with triangular and square rotating units exhibit large stretchability and high ductility in two independent planar directions [27,28]. In addition, auxetic behavior (i.e., negative Poisson's ratio) was observed during the elongation of fractal-cut graphene kirigami [27,29], indicating that numerous known advantages of macroscale kirigami may hold for two-dimensional materials.

Tunability is a known advantage of macroscale kirigami, which enables the design of materials and structures with desirable mechanical properties [30–32]. As a result, kirigami techniques can be used to achieve the required mechanical properties of graphene for targeted applications [33]. Altering the cutting geometry is a simple and effective way to tune the mechanical properties of the graphene kirigami [20]. Particularly, with the aid of machine learning and optimization algorithms, mechanical properties such as fracture strain and stress can be accurately predicted and efficiently tuned [34–36]. Two additional strategies to achieve tunability are the introduction of geometric hierarchies and novel cutting patterns [37,38]. For example, by leveraging these strategies, Cai and Akbarzadeh [27] formulated closed-form analytical algorithms that can predict and tune the stress-strain response of a graphene kirigami.

In addition to parallel and fractal cutting patterns, other cutting patterns can be utilized to achieve stretchable graphene

*Corresponding author: chenyao@seu.edu.cn

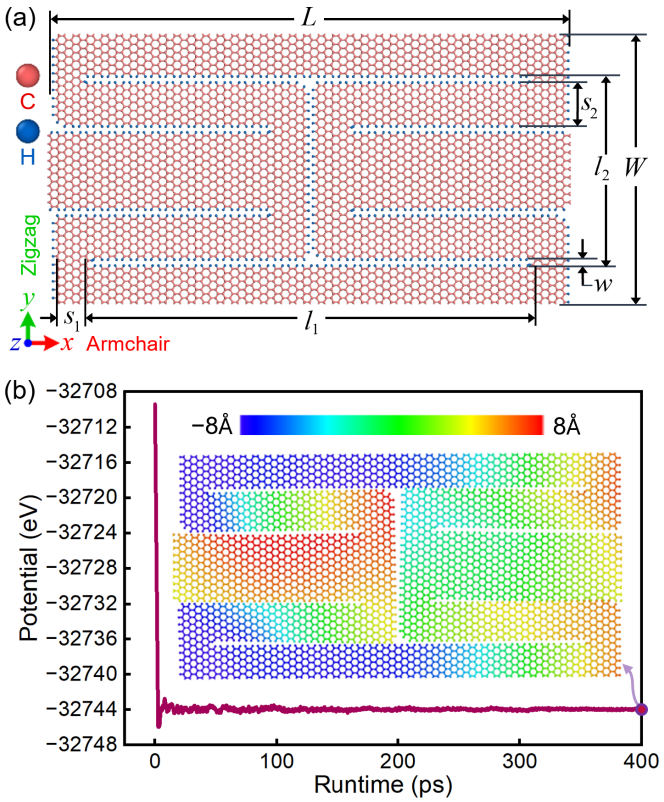

FIG. 1. (a) Atomic morphology of the representative graphene kirigami unit with key geometric parameters labeled. The armchair and zigzag directions of the graphene kirigami are aligned along the x and y axes of the simulation box. (b) The potential energy of the representative unit as a function of simulation time. An out-of-plane displacement contour of the equilibrated structure is depicted in the inset.

kirigami structures with tunable mechanical properties. In this study, we apply an I-shaped cutting pattern, exhibiting large macroscale stretchability and negative Poisson's ratio [39], to monolayer graphene. MD simulations are employed to systematically investigate the tensile response of the proposed graphene kirigami. MD simulations can reflect the evolution of atomic structures during elongation, thereby unveiling the atomic-level failure mechanism of the graphene kirigami. We find that the graphene kirigami exhibits large stretchability and high ductility, as well as negative Poisson's ratios, in two independent planar directions. Furthermore, the stress-strain response of the graphene kirigami can be tuned by altering cutting geometries and connecting various cutting patterns in series. Finally, we develop a numerical algorithm to predict and tune the stress-strain response of the series-connected graphene kirigami structures.

II. MODELS AND METHODS

A. Atomic morphology of the graphene kirigami

Figure 1(a) illustrates the atomic morphology of a representative graphene kirigami unit. This unit was constructed by making I-shaped cuts in a graphene nanoribbon, with the cutting edges stabilized by passivated hydrogen atoms [40]. The cutting geometry is characterized by five parameters: cutting width w, horizontal cutting length l_1, vertical cutting length l_2, and the horizontal and vertical distances between the cuts, denoted by s_1 and s_2, respectively. By periodically replicating this kirigami unit along the two perpendicular planar directions, a multiunit kirigami similar to the original unit can be generated, as detailed in the following.

The representative graphene kirigami unit has geometric parameters of $l_1 \sim 132$ Å, $l_2 \sim 59$ Å, $s_1 \sim 9$ Å, $s_2 \sim 10$ Å, and $w \sim 4$ Å. Our subsequent discussions on the tensile response will be anchored in this particular unit, and trends in the mechanical properties will then be revealed based on parametric analyses. Notably, our primary focus is on graphene kirigami featuring I-shaped cuts parallel to the "zigzag" direction. Nevertheless, MD simulations were also performed on I-shaped cuts parallel to the "armchair" direction to verify the qualitative independence of chirality in the presented results, as described in Supplemental Material S1 [41]. The terms armchair and zigzag are named after the edge shape of graphene, as illustrated in Fig. 1(a).

B. Molecular dynamics simulations

All MD simulations were performed using the large-scale atomic molecular massively parallel simulator, LAMMPS [42]. Atomic interactions were described by the second-generation reactive empirical bond order potential [43], which has been extensively applied to investigate the mechanical properties of carbon nanomaterials [21,29,44,45]. A cut-off radius of 2.0 Å was set for the C-C bond to avoid nonphysical strain hardening effects [46]. Periodic boundary conditions were adopted in the planar directions, while a nonperiodic boundary condition was applied in the out-of-plane direction [27,28,47]. Importantly, the z-direction dimension of the simulation box should be sufficiently large to allow the out-of-plane deformation of graphene kirigami during elongation [28].

In all MD simulations, a temperature of 4.2 K and a time step of 1 fs were employed. To begin with, the system was relaxed by conjugate gradient energy minimization with a tolerance of 10^{-10}. Next, the system was relaxed for 100 ps in the canonical (*NVT*) ensemble, followed by an additional 300 ps in the isothermal-isobaric (*NPT*) ensemble. This simulation time ensured that the system reached equilibrium, as evidenced by the convergence of potential energy in Fig. 1(b). Note that an out-of-plane rippling phenomenon was observed in the equilibrated structure, stemming from the local buckling caused by the artificial cuts [25]. This observation aligns with the reported results on the graphene kirigami featuring diverse cutting patterns [20,27,28,48–50]. Finally, a tensile strain rate of 0.01 ps^{-1} was applied in the armchair or zigzag direction of the system using the deformation-control method [28,51,52]. This particular strain rate could save computational time, and produces a slight effect on the stress-strain response of the graphene kirigami, as shown in Supplemental Material S2 [41].

The tensile process continued until the kirigami structure completely fractured. To account for the Poisson's effect during elongation, we employed the *NPT* ensemble with zero pressure in the direction perpendicular to the tensile direction. Tensile stress was computed as the stress parallel to

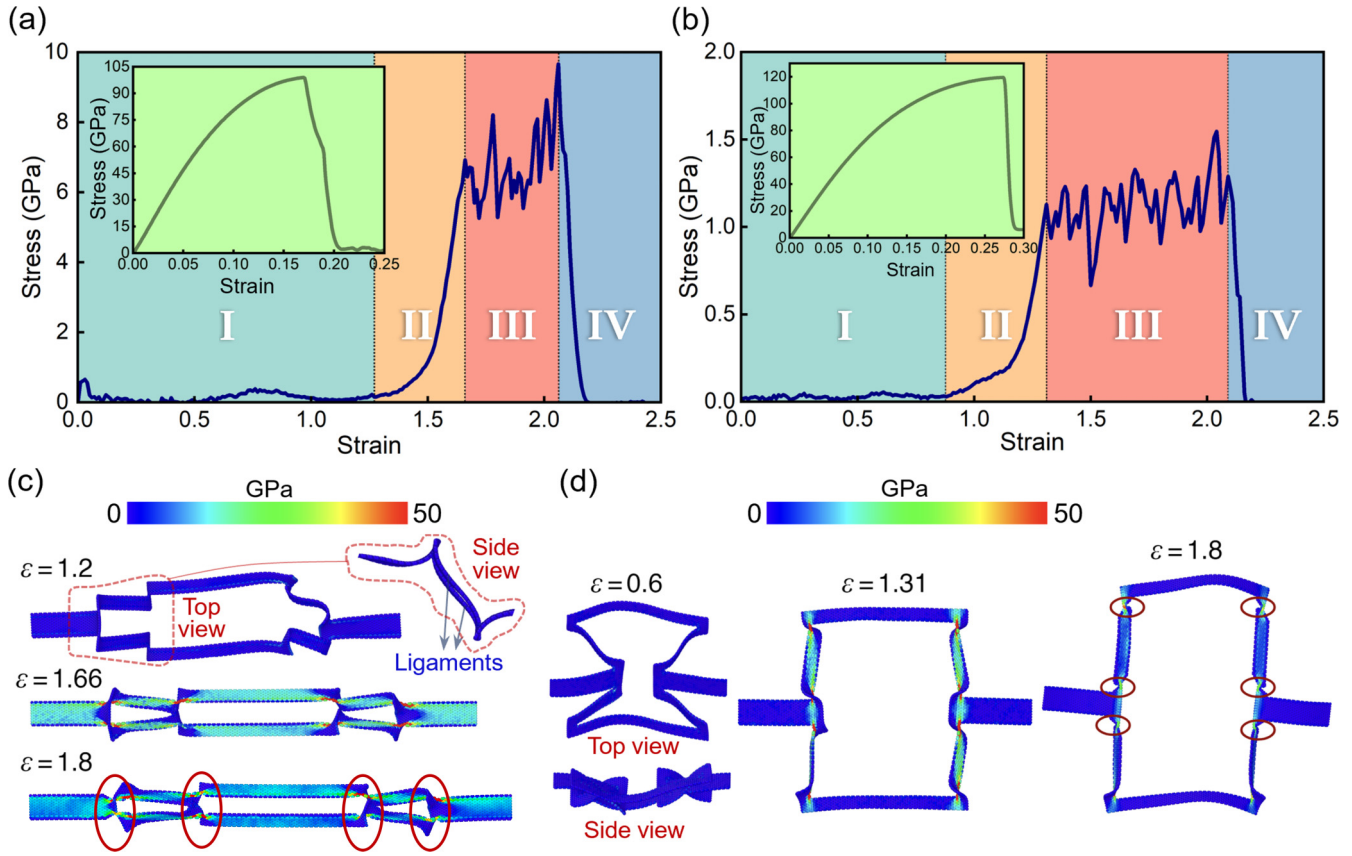

FIG. 2. Uniaxial tensile response of the representative graphene kirigami. (a) Armchair and (b) zigzag stress-strain curves. Four regions, I, II, III, and IV, correspond to four different deformation regimes. The stress-strain curves of a pristine graphene nanoribbon with the same size are depicted in the inset for comparison. Atomic stress contours for the first three deformation regimes under (c) armchair and (d) zigzag tension. $\varepsilon = 1.66$ and $\varepsilon = 1.31$ are the yield strains. Ovals in the inset mark torn ligaments.

the stretching direction, multiplied by the z dimension of the simulation box, and then divided by the graphene effective thickness of 3.35 Å [35]. The computed stress was averaged every 1 ps to establish the stress-strain relationship. Furthermore, atomic trajectories were recorded at an interval of 0.1 ps to visualize the evolution of atomic structures, thereby elucidating the deformation mechanism. The visualization was achieved using the Open Visualization Tool (OVITO) [53].

III. RESULTS AND DISCUSSION

A. Tensile response

We initially examine the uniaxial tensile response of the representative graphene kirigami unit. To elucidate the tensile response, we present the armchair and zigzag stress-strain curves in Fig. 2, as well as the atomic stress contours in the representative deformation regimes. Figures 2(a) and 2(b) illustrate that the uniaxial tensile response of the graphene kirigami is divided into four distinct regimes. In the initial regime, the graphene kirigami undergoes continuous out-of-plane deformation (Fig. S4 [41]), but its stress response is nearly zero, indicating that the C-C bonds are barely stretched. We note that the graphene kirigami exhibits significantly different deformation behaviors under the two stretching schemes. As shown in Fig. 2(c), the cut ligaments under armchair stretching flip out of the plane and align with the stretching direction, while those under zigzag stretching flip out of the plane and rotate around the cut tips [Fig. 2(d)], producing a deformed morphology resembling reentrant honeycomb structures [54–57]. This observation suggests that the I-patterned graphene kirigami exhibits mechanical anisotropy. It should be noted that the deformation mechanism of flipping and rotation plays a crucial role in the large stretchability of the graphene kirigami structure, which will be discussed later.

With the ongoing stretching, atoms around the cut tips progressively yield, initiating the formation of high-stress zones. Concurrently, the interior domains produce obvious mechanical responses, resulting in two stress bands aligned with the stretching direction. As a result, the stress response markedly increases until the entire structure yields, as manifested by the second segment in the stress-strain curves. In this regime, the C-C covalent bonds are elongated, but remain unbroken (Fig. S4 [41]), implying an elastic and reversible deformation in the structure. In comparison with pristine graphene, the yield stress of the graphene kirigami decreases by an order of magnitude, while the armchair and zigzag yield strains increase about ninefold (from 0.17 to 1.66) and fourfold (from 0.28 to 1.31), respectively. The substantial increase in the yield strain signifies a significant enhancement in the stretchability of the graphene kirigami. Moreover, the increment surpasses the reported results of the graphene kirigami featuring parallel cuts [20,21] and fractal cuts [27,28].

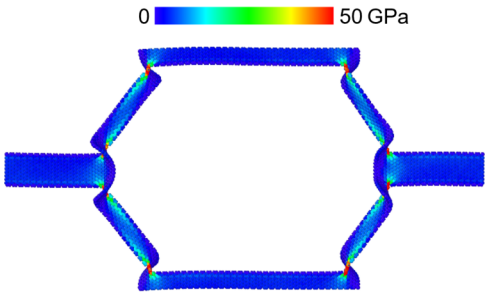

FIG. 3. Atomic stress contour of the representative graphene kirigami unit under biaxial tension at the yield strain of 1.13.

When the flipping and rotation mechanism reaches its limit, the ligaments start to tear at the cut tips. As a result, the C-C covalent bonds around the cut tips rupture, leading to a decline in the stress response. Nevertheless, the newly formed crack surfaces enable the continuation of the flipping and rotation mechanism, causing the stress response to increase again. This process repeatedly proceeds until the structure completely fractures, as evidenced by the zigzag-patterned stress-strain curves in Fig. 2 and the steplike bond-strain curves in Fig. S4. We observe that pristine graphene promptly fractures upon yielding, whereas the armchair and zigzag graphene kirigami demonstrate the ability to endure elongations exceeding 40% and 70%, respectively. This indicates that the I-shaped cutting pattern can impart remarkable ductility to monolayer graphene. The underlying mechanism lies in the flipping and rotation behavior that accompanies ligament tearing.

After demonstrating the high stretchability and ductility of the I-patterned graphene kirigami in two planar directions, we proceed to investigate its deformation response to biaxial tension. Biaxial tensile tests were conducted by simultaneously applying uniform strain rates along the two planar directions of the kirigami structure. Since the planar directions of the system experienced nonzero pressure during biaxial stretching, we employed the *NVT* ensemble. Similar to the results in uniaxial tension, we observe significant enhancements in the stretchability and ductility of the graphene kirigami; that is, the yield strain increases from 0.19 to 1.13, while the structure can undergo over 40% elongation post yielding. The underlying mechanism is similar to that observed in zigzag stretching, i.e., ligament flipping and rotation. Nonetheless, the rotation angle of ligaments in response to biaxial tension surpasses that in the case of zigzag tension, as evidenced by the presence of a hexagonal hole at the yield strain in Fig. 3 and a rectangular hole at the yield strain in Fig. 2(d).

To demonstrate the parallelism in the deformation mechanism between nanoscale graphene kirigami and macroscale kirigami, we fabricated a paper kirigami featuring a similar cutting pattern, and then subjected it to uniaxial and biaxial stretching. As depicted in Fig. 4, the paper kirigami model exhibits deformation behaviors resembling those of the graphene kirigami presented in Figs. 2 and 3. This resemblance implies that some known characteristics of macroscale kirigami may be extended to nanoscale two-dimensional materials. It should be noted that the paper kirigami was not stretched to rupture.

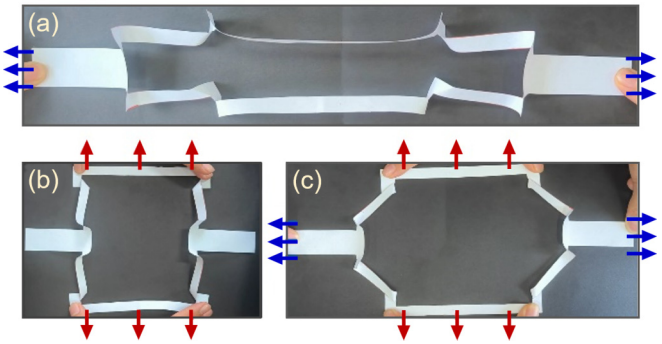

FIG. 4. Top-view pictures of a paper kirigami model with I-shaped cuts. (a) Armchair tension. (b) Zigzag tension. (c) Biaxial tension.

To demonstrate the crucial role of the flipping and rotation mechanism in imparting stretchability to the I-patterned graphene kirigami, we simulated the tensile behavior of the representative kirigami unit without involving out-of-plane deformation. As shown in Fig. 5, the armchair and zigzag yield strains are respectively 0.17 and 0.57, which are approximately 10% and 40% of the values obtained when the out-of-plane deformation is allowed, respectively. Moreover, the kirigami structure without out-of-plane deformation exhibits similar reentrant morphologies during armchair and zigzag stretching. However, as discussed earlier, when out-of-plane deformation is allowed, the kirigami structure manifests anisotropic deformation behaviors. This disparity in deformation is attributed to the flexibility of the single-atom-thick graphene sheet, which shrinks readily during armchair stretching after the ligaments flip to a certain extent. Overall, it is verified that the flipping and rotation mechanism is the predominant factor underpinning the remarkable stretchability of the I-patterned graphene kirigami.

In addition to the graphene kirigami unit detailed previously, we simulated the uniaxial and biaxial tensile responses of a multiple-unit graphene kirigami. The multiple-unit graphene kirigami was constructed by replicating the kirigami unit twice in the armchair direction and thrice in the zigzag direction. As shown in Fig. 6, our results concerning the yield

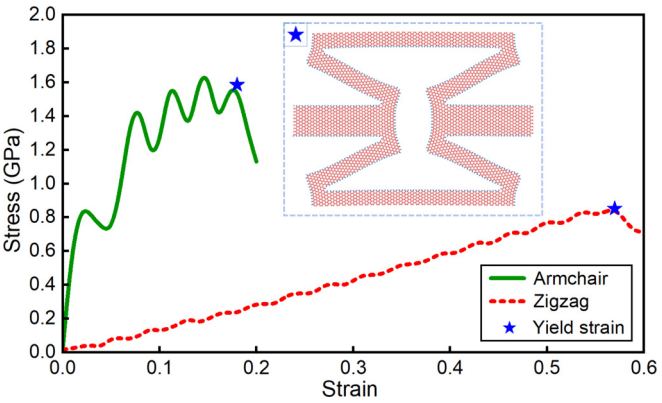

FIG. 5. Uniaxial tensile stress-strain curves of the representative graphene kirigami without out-of-plane deformation. An atomic snapshot at the yield strains is depicted in the inset.

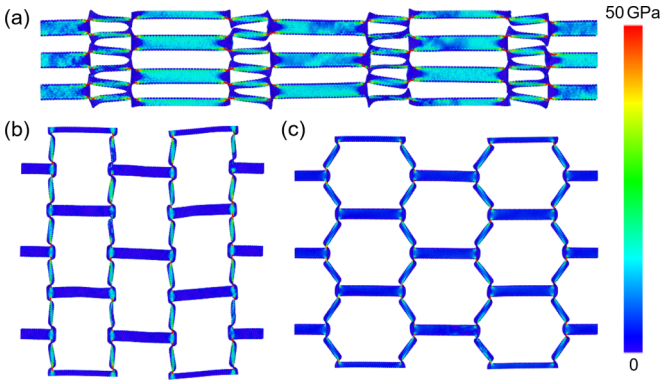

FIG. 6. Atomic stress contours of a multiple-unit graphene kirigami under (a) armchair tension, (b) zigzag tension, and (c) biaxial tension. The displayed morphologies are at the yield strains of 1.63, 1.28, and 1.11, respectively.

and fracture strains, alongside the deformation mechanisms, closely resemble those observed in the single-unit kirigami. This suggests that the tensile response is independent of the number of units. Furthermore, we performed simulations to assess the tensile response of a graphene kirigami featuring cutting geometric parameters twice that of the representative unit. It is found that the yield strain and fracture strain of these two graphene kirigami are very close (more details are presented in Supplemental Material S5 [41]), suggesting that the tensile response is independent of cut size.

B. Negative Poisson's ratio

We observe that the graphene kirigami expands during elongation, indicating negative Poisson's ratios. For a more comprehensive understanding, Fig. 7 depicts the Poisson's ratios of the graphene kirigami as a function of strain. The Poisson's ratios v_{xy} (zigzag) and v_{yx} (armchair) are calculated by $v_{xy} = v_{yx}^{-1} = -\frac{\varepsilon_{xx}}{\varepsilon_{yy}}$, where $\varepsilon_{xx} = \frac{l_x - l_{xo}}{l_x}$ and $\varepsilon_{yy} = \frac{l_y - l_{yo}}{l_y}$. Variables l_x and l_y are the x- and y-direction lengths of the deformed graphene kirigami, respectively, while l_{xo} and l_{yo} are the initial lengths before loading. As can be seen from Fig. 7, the armchair kirigami exhibits varying negative Poisson's ratios until the strain reaches approximately

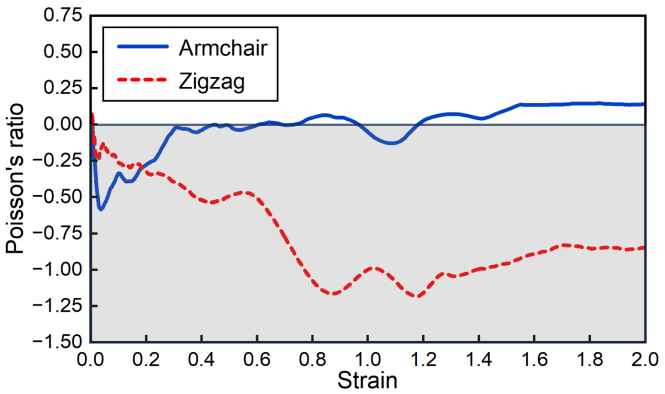

FIG. 7. Poisson's ratio of the representative graphene kirigami unit as a function of strain.

TABLE I. Base values and a full list of values for each parameter.

Parameters (Å)	Base value	All values
l_1	132	98, 115, 141, 149, 158, 166, 175
l_2	59	54, 64, 69, 74, 79, 84, 89
s_1	9	4, 13, 17, 21, 26, 30, 34
s_2	10	5, 7, 12, 15, 17, 20, 22

0.3, beyond which the Poisson's ratio fluctuates around zero and eventually stabilizes at a constant value. Conversely, the zigzag kirigami exhibits consistently changing negative Poisson's ratios throughout the extension, peaking at −1.18, about twice that of the armchair kirigami. By observing the deformation behaviors, we identify that the mechanism leading to negative Poisson's ratios is the rotation of the ligaments relative to the cutting tips during stretching. As previously elucidated, when the ligaments flip to a certain extent, the kirigami structure under armchair stretching easily shrinks in the zigzag direction, causing the rotation mechanism to cease. Consequently, the armchair kirigami does not exhibit a pronounced negative Poisson's ratio after the strain of 0.3. It should be noted that the resulting Poisson's ratio of graphene kirigami is less than the theoretical minimum (−1) for reentrant honeycomb lattices [56,57]. This is mainly because the highly flexible graphene kirigami is not flat before loading, as demonstrated in Fig. 1(b). This means that the calculated strain of rough graphene kirigami is different from that of flat graphene kirigami. On the other hand, due to the buckling of materials around the cutting tips, the graphene kirigami experiences an out-of-plane deformation, while the honeycomb lattice mainly deforms in the plane.

C. Effect of cutting geometry

Having demonstrated the substantial enhancement in the stretchability and ductility of monolayer graphene through the I-shaped cutting pattern, we further study how the cutting geometry shown in Fig. 1(a) impacts the key mechanical properties of interest, namely, the yield strain and fracture strain. Gaining insights into this impact can facilitate the design of graphene kirigami structures with desirable mechanical properties. To this end, we established an additional set of 28 graphene kirigami models and then subjected them to uniaxial tension. The geometric parameters of these models are listed in Table I, with the base values corresponding to the representative graphene kirigami described in Sec. II A. All these kirigami models share a uniform cutting width of 4 Å.

By examining the deformed morphologies in Figs. 2(c) and 2(d), we determine a positive correlation between the elongation of the graphene kirigami structure and the ligament length. More specifically, a larger l_1 or a smaller s_1 results in a longer ligament length. As such, both the yield strain and fracture strain increase with increasing l_1 or decreasing s_1, as demonstrated in Figs. 8(a) and 8(c), respectively. Figure 8(a) shows that the amplitude of variations in the yield and fracture strains under zigzag stretching is larger than that under armchair stretching. This discrepancy arises because the armchair dimension (L) of the graphene kirigami increases

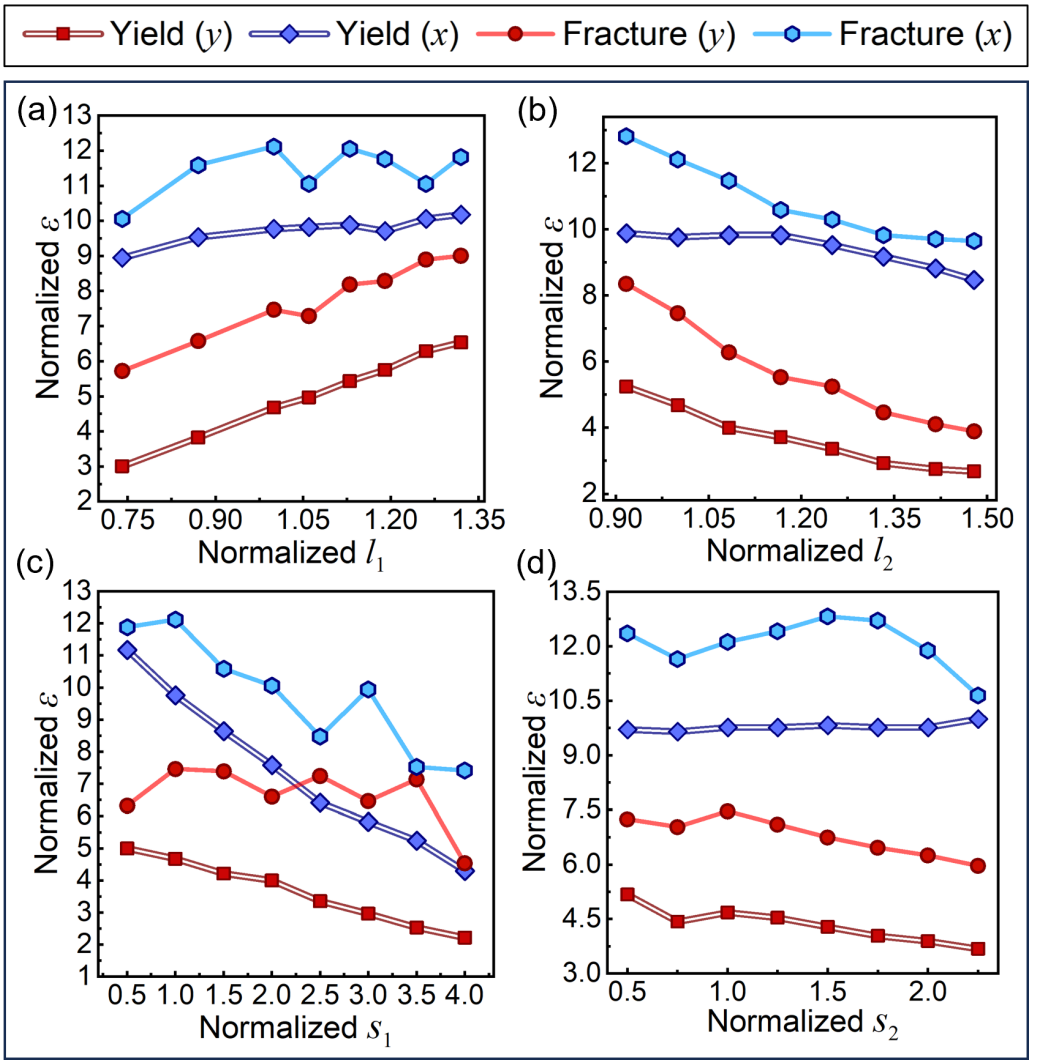

FIG. 8. Effects of (a) l_1, (b) l_2, (c) s_1, and (d) s_2 on the yield strain and the fracture strain of the graphene kirigami under zigzag (y) and armchair (x) tensions. Data for the yield and fracture strains are normalized by simulation results of a pristine graphene nanoribbon of the same size. Data for geometric parameters are normalized by those of the representative graphene kirigami.

with an increase in l_1, whereas the zigzag dimension (W) remains constant. Similarly, increasing l_2 (thus increasing the zigzag dimension) leads to a reduction in the zigzag yield strain and fracture strain, as demonstrated in Fig. 8(b). Note that the armchair yield strain remains relatively stable when l_2 is below 69 Å, after which it exhibits a descending trend. It can be seen from Fig. 8(d) that increasing s_2 has little effect on the armchair yield strain, while causing a modest reduction in the zigzag yield strain. In light of the aforementioned results, we deduce that the kirigami pattern characterized by an increased l_1 value and declined values of l_2, s_1, and s_2 can impart an exceptionally elevated stretchability to nanoscale graphene.

Beyond the adjustable yield strain and fracture strain, the Poisson's ratio of the graphene kirigami can be tuned by altering the geometric parameters of the I-shaped cuts. For instance, increasing l_2 can extend the strain scope of negative Poisson's ratio in the armchair direction; increasing l_1, s_1, or s_2 enhances the peak value of the negative Poisson's ratio in the zigzag direction, while increasing l_2 yields the opposite effect (more details are presented in Supplemental Material S6 [41]).

D. Tunable stress-strain response

After investigating the impact of cutting geometry on the tensile response of the I-shaped graphene kirigami, we proceed to design series-connected graphene kirigami structures (i.e., interlinking different kirigami patterns in series) and develop a numerical algorithm to predict their mechanical behavior. We primarily consider the graphene kirigami featuring cutting patterns interconnected along the zigzag direction depicted in Fig. 1(a). Upon subjecting the series-connected kirigami to uniaxial tensile strain along the zigzag direction, the nominal stress is identical in all n constituent building blocks [38], denoted as

$$\sigma_s = \sigma_{\#i} = \cdots = \sigma_{\#n}, \tag{1}$$

where σ_s is the nominal stress in the series-connected kirigami, and $\sigma_{\#i}$ denotes the stress of the ith building block.

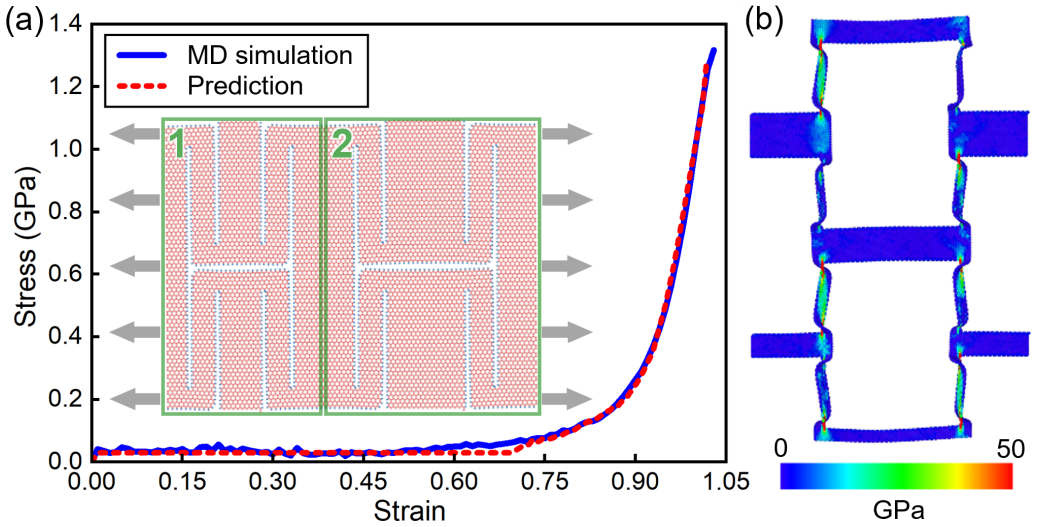

FIG. 9. Tensile response of series-connected graphene kirigami consisting of two building blocks. (a) Stress-strain curves as predicted by the analytical model and MD simulations. Atomic morphology before stretching is depicted in the inset. (b) Atomic stress contour at the yield strain.

Given the independence of elongation in individual building blocks, the total elongation of the structure is achieved by summing the elongations of each respective building block [38]. As such, the strain of the series-connected kirigami can be expressed as

$$\varepsilon_s = \sum_{i=1}^{i=n} \frac{\varepsilon_{\#i} L_{\#i}}{L_s}, \tag{2}$$

where ε_s, σ_s, and $L_s = \sum_{i=1}^{i=n} L_{\#i}$ represent the strain, stress, and initial length of the series-connected kirigami, respectively; and $\varepsilon_{\#i}$, $\sigma_{\#i}$, and $L_{\#i}$ denote the strain, stress, and initial length of the ith building block, respectively. It should be noted that the initial length corresponds to the length after the relaxation process. Thus, by utilizing Eqs. (1) and (2) with the stress-strain curves obtained for each building block via the MD simulation as input, we can straightforwardly predict the stress-strain response of the series-connected kirigami. For ease of computation, the stress in the first deformation regime is averaged, and the post-yield stress data are ignored (more details can be found in Supplemental Material S7 [41]).

Figure 9(a) illustrates a series-connected graphene kirigami structure consisting of two different kirigami patterns. Kirigami 1 corresponds to the previously described representative structure, while kirigami 2 retains the same geometric parameters as kirigami 1, differing solely in l_2, which is 79 Å. As can be seen from Fig. 9(a), the predicted stress-strain curve demonstrates a reasonable agreement with the MD simulation. This correspondence implies the reliability of the developed numerical algorithm in accurately predicting the tensile response of series-connected graphene kirigami structures, provided that the stress-strain relationships of individual building blocks are obtained. Moreover, as shown in Fig. 9(b), the tensile deformation behavior of each building block in this series-connected graphene kirigami exhibits a resemblance to the corresponding deformation behavior shown in Fig. 2(d). In addition, we simulated the tensile response of a series-connected kirigami structure comprising three different kirigami patterns, detailed in Supplemental Material S7 [41].

Based on the developed numerical algorithm, the stress-strain response of series-connected kirigami structures can be predicted as long as the stress and strain relationships of each building block are known. In addition, the stress-strain response of these structures can be tuned by altering the cutting geometry or by increasing the number of building blocks. Importantly, the computational costs of MD simulations increase exponentially with the size of the sysetem. This approach facilitates the rapid design of graphene kirigami with desirable stress-strain response while saving considerable computational costs.

IV. CONCLUSIONS

In this study, we have utilized MD simulations to systematically investigate the tensile response of monolayer graphene kirigami structures featuring an I-shaped cutting pattern. Our results reveal that the graphene kirigami exhibits exceptional stretchability and ductility in two planar directions due to the flipping and rotation mechanism of the ligaments during elongation. The yield strain and fracture strains can experience an approximately 6-fold and 9-fold increase in one direction, and about a 10-fold and 12-fold increase in the other direction, respectively. In addition, the graphene kirigami exhibits negative Poisson's ratios, attributed to the ligament rotation during elongation. Notably, the zigzag kirigami has negative Poisson's ratios with a smaller extremum and a longer strain range compared to the armchair kirigami. This disparity arises from the disappearance of the rotation mechanism, a consequence of the armchair graphene shrinking in the zigzag direction.

Based on the conducted parametric analyses, we discern that the yield strain and fracture strain of the graphene

kirigami structure can be tuned by altering the cutting geometries. To be specific, increasing the horizontal cutting length (l_1) or reducing the vertical cutting length (l_2) and the distances between the cuts (s_1 and s_2) enhances the stretchability of the graphene kirigami. The extremum and strain range of negative Poisson's ratios can also be tailored by altering the geometric parameters. Furthermore, we ascertain that the stress-strain response of the graphene kirigami can be tuned by connecting alternative kirigami building blocks in series. We have developed a numerical algorithm capable of effectively predicting and tuning the stress-strain response of the series-connected graphene kirigami. On this basis, we can proceed to design graphene kirigami structures with desirable stress-strain responses. These findings are expected to advance our understanding and the applications of programmable kirigami nanomaterials. The proposed highly stretchable and ductile graphene kirigami may open new avenues for flexible electronics such as stretchable electrodes [58], strain sensors [59–62], and hydroelectric generators [63].

ACKNOWLEDGMENTS

This work has been supported by the National Natural Science Foundation of China (Grant No. 51978150), the Natural Science Foundation of Jiangsu Province for Distinguished Young Scientists (Grant No. BK20231517), and the Postgraduate Research and Practice Innovation Program of Jiangsu Province (SJCX23_0071). Y.C. would like to acknowledge financial support from the Alexander von Humboldt Foundation for his academic research at Max-Planck-Institut für Eisenforschung GmbH, Germany. The authors are grateful to the anonymous reviewers for their constructive comments and suggestions.

[1] A. K. Geim and K. S. Novoselov, Nat. Mater. **6**, 183 (2007).
[2] C. Lee, X. Wei, J. W. Kysar, and J. Hone, Science **321**, 385 (2008).
[3] A. A. Balandin, S. Ghosh, W. Z. Bao, I. Calizo, D. Teweldebrhan, F. Miao, and C. N. Lau, Nano Lett. **8**, 902 (2008).
[4] Y. B. Zhang, Y. W. Tan, H. L. Stormer, and P. Kim, Nature (London) **438**, 201 (2005).
[5] H. B. Heersche, P. Jarillo-Herrero, J. B. Oostinga, L. M. K. Vandersypen, and A. F. Morpurgo, Nature (London) **446**, 56 (2007).
[6] M. D. Stoller, S. Park, Y. Zhu, J. An, and R. S. Ruoff, Nano Lett. **8**, 3498 (2008).
[7] C. Y. Chen, S. Rosenblatt, K. I. Bolotin, W. Kalb, P. Kim, I. Kymissis, H. L. Stormer, T. F. Heinz, and J. Hone, Nat. Nanotechnol. **4**, 861 (2009).
[8] A. Voje, J. M. Kinaret, and A. Isacsson, Phys. Rev. B **85**, 205415 (2012).
[9] F. Liu, P. M. Ming, and J. Li, Phys. Rev. B **76**, 064120 (2007).
[10] M. Xu, J. T. Paci, J. Oswald, and T. Belytschko, Int. J. Solids Struct. **49**, 2582 (2012).
[11] H. Zhao, K. Min, and N. R. Aluru, Nano Lett. **9**, 3012 (2009).
[12] H. Jang, Y. J. Park, X. Chen, T. Das, M. S. Kim, and J. H. Ahn, Adv. Mater. **28**, 4184 (2016).
[13] M. K. Blees *et al.*, Nature (London) **524**, 204 (2015).
[14] K. Yong, S. De, E. Y. Hsieh, J. Leem, N. R. Aluru, and S. Nam, Mater. Today **34**, 58 (2020).
[15] C. Dai *et al.*, Nano Lett. **22**, 5301 (2022).
[16] T. C. Shyu, P. F. Damasceno, P. M. Dodd, A. Lamoureux, L. Xu, M. Shlian, M. Shtein, S. C. Glotzer, and N. A. Kotov, Nat. Mater. **14**, 785 (2015).
[17] M. Isobe and K. Okumura, Phys. Rev. Res. **1**, 022001(R) (2019).
[18] M. Isobe and K. Okumura, Sci. Rep. **6**, 24758 (2016).
[19] S. H. Chen, K. C. Chan, T. M. Yue, and F. F. Wu, Scr. Mater. **142**, 83 (2018).
[20] Z. Qi, D. K. Campbell, and H. S. Park, Phys. Rev. B **90**, 245437 (2014).
[21] Z. Hua, Y. Zhao, S. Dong, P. Yu, Y. Liu, N. Wei, and J. Zhao, Soft Matter **13**, 8930 (2017).
[22] N. Wei, Y. Chen, K. Cai, J. Zhao, H. Wang, and J. Zheng, Carbon **104**, 203 (2016).
[23] E. Jalali, H. Soltanizadeh, Y. Chen, Y. M. Xie, and P. Sareh, Commun. Mater. **3**, 97 (2022).
[24] Y. Chen, W. Ye, R. Xu, Y. Sun, J. Feng, and P. Sareh, Int. J. Mech. Sci. **249**, 108249 (2023).
[25] A. Rafsanjani and K. Bertoldi, Phys. Rev. Lett. **118**, 084301 (2017).
[26] K. A. Seffen, Phys. Rev. E **94**, 033003 (2016).
[27] J. Cai and A. Akbarzadeh, Mater. Des. **206**, 109811 (2021).
[28] P. Shi, Y. Chen, Y. Wei, J. Feng, T. Guo, Y. Tu, and P. Sareh, Phys. Rev. B **108**, 134105 (2023).
[29] V. H. Ho, D. T. Ho, S. Kwon, and S. Y. Kim, Phys. Status Solidi B **253**, 1303 (2016).
[30] Y. Sun, W. Ye, Y. Chen, W. Fan, J. Feng, and P. Sareh, Structures **33**, 3633 (2021).
[31] J. Tao, H. Khosravi, V. Deshpande, and S. Li, Adv. Sci. **10**, 2204733 (2023).
[32] Z. Zhai, L. Wu, and H. Jiang, Appl. Phys. Rev. **8**, 41319 (2021).
[33] S. Hong, H. Lee, J. Lee, J. Kwon, S. Han, Y. D. Suh, H. Cho, J. Shin, J. Yeo, and S. H. Ko, Adv. Mater. **27**, 4744 (2015).
[34] P. Rajak, B. Wang, K. Nomura, Y. Luo, A. Nakano, R. Kalia, and P. Vashishta, npj Comput. Mater. **7**, 102 (2021).
[35] P. Z. Hanakata, E. D. Cubuk, D. K. Campbell, and H. S. Park, Phys. Rev. Lett. **121**, 255304 (2018).
[36] P. Z. Hanakata, E. D. Cubuk, D. K. Campbell, and H. S. Park, Phys. Rev. Res. **2**, 042006(R) (2020).
[37] Y. Tang and J. Yin, Extreme Mech. Lett. **12**, 77 (2017).
[38] N. An, A. G. Domel, J. Zhou, A. Rafsanjani, and K. Bertoldi, Adv. Funct. Mater. **30**, 1906711 (2020).
[39] L. Mizzi, K. M. Azzopardi, D. Attard, J. N. Grima, and R. Gatt, Phys. Status Solidi RRL **9**, 425 (2015).
[40] H. Ghasemi, A. Rajabpour, and A. H. Akbarzadeh, Int. J. Heat Mass. Transfer **123**, 261 (2018).
[41] See Supplemental Material at http://link.aps.org/supplemental/10.1103/PhysRevE.109.035002 for details on the effects of graphene chirality, sample size, and strain rate on the tensile

response of graphene kirigami. It also shows the formation of sp^2 bonds during relaxation, the average out-of-plane displacement and number of C–C bonds during elongation, the effect of cutting geometry on Poisson's ratio, and the detailed disccussion on the tunable stress-strain response.

[42] A. P. Thompson *et al.*, Comput. Phys. Commun. **271**, 108171 (2022).

[43] D. W. Brenner, O. A. Shenderova, J. A. Harrison, S. J. Stuart, B. Ni, and S. B. Sinnott, J. Phys.: Condens. Matter **14**, 783 (2002).

[44] P. Zhang *et al.*, Nat. Commun. **5**, 3782 (2014).

[45] Y. Zhao, C. Wang, J. Wu, C. Sui, S. Zhao, Z. Zhang, and X. He, Phys. Chem. Chem. Phys. **19**, 11032 (2017).

[46] O. A. Shenderova, D. W. Brenner, A. Omeltchenko, X. Su, and L. H. Yang, Phys. Rev. B **61**, 3877 (2000).

[47] P. Shi, Y. Lin, T. Guo, M. Fang, C. Wang, Y. Tu, G. Sas, and L. Elfgren, J. Mater. Civ. Eng. **35**, 4023232 (2023).

[48] B. Zheng and G. X. Gu, Carbon **155**, 697 (2019).

[49] B. F. Grosso and E. J. Mele, Phys. Rev. Lett. **115**, 195501 (2015).

[50] D. A. Bahamon, Z. Qi, H. S. Park, V. M. Pereira, and D. K. Campbell, Phys. Rev. B **93**, 235408 (2016).

[51] N. Wei, L. Xu, H. Wang, and J. Zheng, Nanotechnology **22**, 105705 (2011).

[52] Y. Tu, P. Shi, D. Liu, R. Wen, Q. Yu, G. Sas, and L. Elfgren, Phys. Chem. Chem. Phys. **24**, 1156 (2022).

[53] A. Stukowski, Model. Simul. Mater. Sci. Eng. **18**, 15012 (2010).

[54] H. Yasuda and J. Yang, Phys. Rev. Lett. **114**, 185502 (2015).

[55] X. Cheng, Y. Zhang, X. Ren, D. Han, W. Jiang, X. G. Zhang, H. C. Luo, and Y. M. Xie, Int. J. Mech. Sci. **223**, 107286 (2022).

[56] L. J. Gibson, M. F. Ashby, G. S. Schajer, and C. I. Robertson, Proc. R. Soc. A **382**, 25 (1982).

[57] R. S. Lakes, Annu. Rev. Mater. Res. **47**, 63 (2017).

[58] W. Zheng *et al.*, Chem. Mater. **30**, 6063 (2018).

[59] E. Okogbue *et al.*, Nano Lett. **19**, 7598 (2019).

[60] C. Lu, Y. Chen, J. Yan, J. Feng, and P. Sareh, J. Mech. Robot. **16**, 031001 (2024).

[61] Y. Chen, C. Lu, W. Fan, J. Feng, and P. Sareh, Thin Wall Struct. **185**, 110626 (2023).

[62] K. Xu, Y. Lu, S. Honda, T. Arie, S. Akitaa, and K. Takei, J. Mater. Chem. C **7**, 9609 (2019).

[63] C. Yang, Y. Huang, H. Cheng, L. Jiang, and L. Qu, Adv. Mater. **31**, 1805705 (2019).